Food & Function

Accepted Manuscript

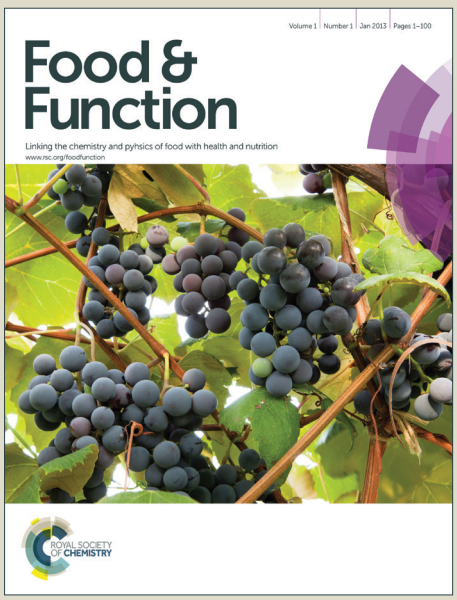

This is an *Accepted Manuscript*, which has been through the Royal Society of Chemistry peer review process and has been accepted for publication.

Accepted Manuscripts are published online shortly after acceptance, before technical editing, formatting and proof reading. Using this free service, authors can make their results available to the community, in citable form, before we publish the edited article. We will replace this *Accepted Manuscript* with the edited and formatted *Advance Article* as soon as it is available.

You can find more information about *Accepted Manuscripts* in the Information for Authors.

Please note that technical editing may introduce minor changes to the text and/or graphics, which may alter content. The journal's standard Terms & Conditions and the Ethical guidelines still apply. In no event shall the Royal Society of Chemistry be held responsible for any errors or omissions in this *Accepted Manuscript* or any consequences arising from the use of any information it contains.

ROYAL SOCIETY OF CHEMISTRY

www.rsc.org/foodfunction

Deciphering the binding patterns and conformation changes upon the bovine serum albumin-rosmarinic acid complex

Xin Peng,‡[ab] Xiangchao Wang, ‡[b] Wei Qi,*[bcde], Renliang Huang,[f] Rongxin Su[bcde] and Zhimin He[bc]

[a]School of Life Sciences, Tianjin University, Tianjin 300072, PR China

[b]Chemical Engineering Research Center, School of Chemical Engineering and Technology, Tianjin University, Tianjin 300072, PR China

[c]State Key Laboratory of Chemical Engineering, Tianjin University, Tianjin 300072, PR China

[d]Collaborative Innovation Center of Chemistry Science and Engineering (Tianjin), Tianjin 300072, PR China

[e]Tianjin Key Laboratory of Membrane Science and Desalination Technology, Tianjin, 300072, PR China

[f]School of Environmental Science and Engineering, Tianjin University, Tianjin 300072, PR China

---

‡ These authors contributed equally to this work.

† Electronic supplementary information (ESI) available.

*Corresponding author: Wei Qi

Address: Chemical Engineering Research Center, School of Chemical Engineering and Technology, Tianjin University, Tianjin 300072, PR China

Tel: +86-22-27407799

Fax: +86-22-27407599

E-mail: qiwei@tju.edu.cn (W. Qi)

Rosmarinic acid (RA) is an importantly and naturally occurring polyphenol from plants of the mint family with potent biological activities. Here, the *in vitro* interaction of RA with bovine serum albumin (BSA) has been investigated, using various biophysical approaches as well as molecular modeling methods, to ascertain its binding mechanism and conformational changes. The fluorescence results demonstrated that the fluorescence quenching of BSA by RA was mainly the result of the formation of a ground state BSA-RA complex, and BSA had one high affinity RA binding site with binding constant 4.18×10^4 mol L^{-1} at 298 K. Analysis of thermodynamic parameters revealed that hydrophobic and hydrogen bond interactions were the dominant intermolecular force in the complex formation. The primary binding site of RA in BSA (site I) had been identified by site marker competitive experiments. The distance between RA and the tryptophan residue of BSA was evaluated at 3.12 nm based on the Förster's theory of non–radiation energy transfer. The UV-vis absorption, synchronous fluorescence, three-dimensional fluorescence, 8-anilino-1-naphthalenesulfonic acid fluorescence (ANS), circular dichroism (CD), and Fourier transform infrared (FT-IR) spectra confirmed that the conformation and structure of BSA was altered in the presence of RA. Moreover, the nuclear magnetic spectroscopy showed that the aromatic groups of RA took part in the binding reaction during the BSA-RA complexation. In addition, the molecular picture of interaction mechanism between BSA and RA at the atomic level was well examined by molecular docking and dynamics studies. In brief, RA can bind to BSA with noncovalent bond in a relatively stable way, and these findings will be beneficial to the functional food research of RA.

Introduction

In recent years, plenty of natural polyphenol compounds have been isolated from a variety of fruit, vegetable and spice sources, due to their beneficial effects to improve human health[1]. Among these polyphenols, rosmarinic acid (RA) (Fig. 1), an ester of caffeic acid and 3,4-dihydroxyphenyl lactic acid, is an important group of phenolic substance. It has numerous biological and pharmacological activities, such as antioxidant, antiallergic, antimicrobial, antibacterial and anti-inflammatory[2,3]. Moreover, RA is also potentially valuable for improvement of diabetes mellitus and obesity by inhibiting digestive enzymes, such as α-amylase and α-glucosidase[4]. Although RA shows many potent beneficial activities, the possible benefits can be influenced by the bioavailability and transport of RA. Hence, information about these properties of RA is required to investigate. The absorption, metabolism and excretion behaviors of RA have been studied in some previous papers[5,6]. However, little is known about the transport and distribution of RA to target tissue via the circulatory system, which can be affected by the binding of serum albumin. When RA is transferred to tissue through the blood system, there exists an equilibrium between free RA and protein-bound RA, but only the free drug exerts efficacy. Therefore, the interaction mechanism between RA and serum albumin must be investigated to determine the availability of RA *in vivo*.

Fig. 1

It is well known that the transportation of compounds is generally accessed by binding to carrier proteins in plasma. Being the most abundant carrier proteins in blood plasma, serum albumin plays a vital role in the transportation of various exogenous and endogenous substances such as fatty acids, amino acids, certain metals, drugs and nutrients[7]. Here, bovine serum albumin (BSA) is employed as a model

protein because of its medical importance, low cost, ready availability and especially due to structural similarity with human serum albumin (HSA)[8]. In fact, the tertiary structure of BSA is about 76% similar to that of HSA. BSA is a large globular protein with 583 amino acid residues and consists of three homologous domains (I-III) which are divided into 9 loops connected by 17 disulfide bonds[9]. BSA has two tryptophan residues (Trp-134 and Trp-212) that possess intrinsic fluorescence. The former is located on the hydrophilic surface of the protein in subdomain IB, whereas the latter is buried in a hydrophobic pocket of the subdomain IIA, which corresponds to the so-called Sudlow I binding site[10].

It is widely assumed today that the binding of small ligands to proteins by noncovalent interactions is fundamental to many biological processes, and this procedure is an indispensable factor that significantly affects the distribution, duration, metabolism and excretion properties of a drug[11,12]. Thus, it is of great interest to explore the interaction mechanism of protein-drug complexation, and a large number of ligand-binding studies involving HSA or BSA were carried out until now[13-15]. There had been some studies to study the interaction of RA to BSA. Skrt et al.[16] reported the interaction of RA to BSA using fluorescence spectra, CD method and molecular docking at pH 7.5 and calculated the fluorescence quenching parameters (Stern-Volmer quenching constant, biomolecular quenching constant and modified Stern-Volmer quenching constant) for the interaction process, however, no detailed discussion on the binding constants and the nature of force involving in the interaction of RA with BSA was reported. In another study, the interaction between BSA and RA was examined by fluorescence quenching and UV-vis absorption spectra[17], but because RA exhibited exponential dependence in the Stern-Volmer diagram of the BSA-RA system and for this reason the BSA-RA system was not studied in the

overall assessment of binding mechanism[17]. Most importantly, these studies are insufficient in terms of elimination of the inner filter effect, site marker competitive experiments, NMR experiments and molecular modelling, which were of great importance for perfectly demonstrating the interaction of RA with protein. Thus, an accurate and full basic data for clarifying the interaction mechanisms and noncovalent binding process between RA and BSA at molecular level remained unclear and was worthy of being disclosed.

This study was designed to research a new array on the interaction between RA and BSA *in vitro*. In the present work, the interaction between RA and BSA was studied under simulative physiological conditions using a multispectroscopic method consisting of UV-vis absorption, fluorescence, FT-IR, CD and NMR spectroscopy, in combination with computational approaches for the first time, and the result of each method was compatible and complemented one another. The binding mechanism of RA to BSA regarding to quenching mechanism, binding constant, the number of binding sites, binding distance, thermodynamic parameter, and the conformational change of BSA were investigated in detail. Meanwhile, the site marker competitive experiments were also performed to determine the primary binding site of RA on BSA. In addition, the docking and molecular dynamic simulation methods were used to understand the molecular picture of binding, which corroborated with the experimental results. The results can give us a better understanding of the dynamic behavior of RA and may also provide useful information for the design of the analogues with effectively functional properties.

Experimental

Materials

BSA (≥98%), ibuprofen and 8-anilino-1-naphthalenesulfonic acid fluorescence (ANS)

were purchased from Sigma–Aldrich Corp (Shanghai, China) and used without further purification. Rosmarinic acid (≥97%, analytical standard, RA), warfarin and digitoxin were obtained from Aladdin Reagent Co., Ltd. (Shanghai, China). The average molecular weight of BSA was assumed as 66000 g mol^{-1} for calculations. The stock solutions of BSA (1.0×10^{-5} mol L^{-1}) were directly dissolved in phosphate buffer (concentration: 0.02 mol L^{-1}, pH: 7.4, NaCl: 0.1 mol L^{-1}) and were kept in a refrigerator at 4 °C. RA solution (1.0×10^{-4} mol L^{-1}) was prepared by dissolving appropriate amount in phosphate buffer solution. All other reagents used were of analytical purity or higher. The deionized water was produced by a Milli-Q Ultrapure Water Purification System from Millipore (Billerica, MA, USA). Appropriate blanks, run under the same conditions, were subtracted from the sample spectra. The reported pH measurements were carried out with a digital pH-meter with a combined glass-calomel electrode. All solutions were thoroughly degassed before use.

Fluorescence spectroscopy

Fluorescence spectra were carried out on FluoroLog 3 spectrofluorimeter (Horiba Jobin Yvon Scientific, America) equipped with a 1.0 cm path-length quartz cell and a circulating water bath. The widths of both the excitation slit and the emission slit were set at 2.0 nm for all the measurements. 280 nm has been chosen as excitation wavelength, and the emission fluorescence were obtained from 290 to 500 nm. BSA solution (5.0×10^{-6} mol L^{-1}) was titrated with RA (0 to 6.0×10^{-5} mol L^{-1}) at three different temperatures (288, 298 and 308 K). Titrations were done manually by using trace syringe. All solutions were mixed thoroughly and kept 10 min before measurements.

The site marker competitive experiments were performed at 298 K using three different site markers, warfarin for site I, ibuprofen for site II, and digitoxin for site III.

Three milliliters of BSA-RA mixture solution (BSA: 5.0×10^{-6} mol L^{-1}, RA: 2.0×10^{-5} mol L^{-1}) was added to a quartz cell. Then the site marker stock solution were successively added to the mixture solution to obtain an overall site marker concentration ranging from 5 to 40.0×10^{-6} mol L^{-1}. The fluorescence spectra were recorded in the range of 290−500 nm upon excitation at 280 nm.

Time-resolved fluorescence spectra were collected by a time-correlated single photon counting (TCSPC) setup from IBH Horiba Jobin Yvon (USA) with excitation wavelength of 295 nm. The analysis of lifetime was obtained by IBH DAS6 analysis software, and the data were analyzed via a deconvolution method and fitted with a multi-exponential decay function. The quality of each fitting was judged by χ^2 values and visual inspection of the residuals of the fitted function to the data.

Synchronous fluorescence spectroscopy was recorded to investigate the conformational changes of protein at 298 K, while $\Delta\lambda$ (λem-λex) were set at 15 and 60 nm, and the fluorescence spectra were recorded in the wavelength range, 260-320 nm.

Three-dimensional fluorescence measurements were measured on Cary Eclipse Spectrofluorimeter (Varian corporate, USA) equipped with 1.0 cm quartz cells at the following conditions: the emission wavelength was recorded from 200 nm to 360 nm; the excitation wavelength was recorded at 230-550 nm.

BSA (5.0×10^{-6} mol L^{-1}) was incubated at 277 K for a night in the absence or presence of proper concentrations of RA, then ANS (1.5×10^{-5} mol L^{-1}) was added and reacted for 10min at 310 K in a thermostat bath. Binding of ANS to BSA was performed at 298 K using excitation at 370 nm and measuring the emission fluorescence spectra between 400 and 600 nm.

UV–vis absorption spectroscopy

The UV–vis absorption spectra were recorded at room temperature on a TU–1810SPC

spectrophotometer (Puxi Analytic Instrument Ltd. Of Beijing, China) equipped with a 1.0 cm path length cell. The samples were incubated for 30min and the spectra were recorded in the range of 200-500 nm.

Fourier transform infrared (FT-IR) spectroscopy

FT-IR measurements were carried out at room temperature on a Bruker Vertex 70 FT-IR spectrometer (Bruker, Ettlingen, Germany) via the ATR method with a resolution of 4 cm^{-1} and 60 scans. The concentrations for BSA and RA for the FT-IR spectra analysis were 1.0×10^{-4} mol L^{-1} and 4.0×10^{-4} mol L^{-1}, respectively. For the FT-IR spectra of BSA (in free form), the absorbance of buffer solution was firstly measured, and then digitally subtracted from that of the protein solution to get the spectrum of the protein alone. For the BSA-RA system in buffer solution (in binding form), the same procedure was performed except that a RA buffer solution with the same concentration as in BSA-RA solution was used as a background.

Circular dichroism spectroscopy

Far-UV (200-260 nm) and near-UV (260-320 nm) CD measurements of BSA/RA samples were recorded on a J–810 CD spectrometer (JASCO, Japan) at room temperature in nitrogen atmosphere when the slit width was set at 1 nm. Each spectrum presented was the average of three consecutive scans with a scan speed of 100 nm/min when the response time was set to 1 s. Quartz cuvettes of path lengths 2 mm and 10 mm were used for the far-UV and near-UV regions, respectively. The concentration of BSA used was 2.5×10^{-6} mol L^{-1} in the far-UV and 1×10^{-5} mol L^{-1} in the near-UV range. An ellipticity of CD spectra was expressed in milli-degrees. Appropriate buffer solution running under the same conditions were taken as blank and subtracted from sample spectra.

Nuclear magnetic resonance (NMR) measurements

The NMR spectra experiments were collected on a Varian Inova 500 MHz Spectrometer (USA) with 32,000 data points, 1200 Hz spectral width, 3.4 s acquisition, and 3 s relaxation delay. Solutions of BSA and RA were prepared using a 0.02 mol L^{-1} phosphate buffer (pH 7.4) in D_2O. The finally molar ratios of RA and BSA measured were set at 1:0, 100:1 and 10:1. All the NMR spectra were performed at 298 K.

Molecular docking

To evaluate the potential interaction of ligand and the protein at the atomic level, the CDOCKER algorithm in the Discovery Studio 2.5 environment was used in this study. The crystal structure of the BSA was obtained from the RCSB Protein Data Bank (PDB code: 4JK4). All the water molecules in BSA were removed, the hydrogen atoms were added and partial charges were assigned based on CHARMm force field at the desired pH of 7.4[18]. The ligand structure was extracted from the crystal structure of PrTX-I complexed to Rosmarinic Acid (PDB code: 3QNL). The parameters were at their default setting in the docking tab, and the grid maps were constructed adequately large to include the binding sites of BSA as well as significant regions of the surrounding surface. BSA was rigid, whereas the ligand was flexible during the docking process under optimum settings[18]. After molecular docking, conformation on the lowest CDOCKER interaction energy pose was selected as the most probable binding conformation.

Molecular dynamics simulations

Once the ligand has been docked into the binding site, a molecular dynamic (MD) simulation was performed using NAMD 2.9 software package. The system was centered in a cubic box of TIP3P water molecules[19]. A sufficient number of Na^+ ions were added to neutralize the negative charges in the system. The ff99SB force field

was used to assign protein, with general Amber force field (GAFF) parameterized for substrate. The system was first minimized by 5000 steps of steepest and 5000 steps of conjugate gradient. Then the system was heated to the target temperature of 300 K for a period of 20 ps in constant pressure periodic boundary conditions (NPT). After that, the system was subjected to equilibrate the system by 5 ns of constant pressure and temperature (NPT) with a time step of 1fs, which was followed by 6 ns of production simulation performed in the same conditions. A cutoff of 14 Å was used for non-bonded interactions and long-range electrostatic interactions were treated by means of the Particle Mesh Ewald (PME) method[20]. The MD simulation results were analyzed using the ptraj program in the AmberTools 14 package and Visual Molecular Dynamics (VMD) 1.9.1.

Results and discussion

Elimination of the inner filter effect

In the fluorescence experiment, although RA had insignificant absorption at excitation and emission wavelengths of BSA, it can lead to an obvious decrease in fluorescence intensity that was an inner filter effect[21,22]. Hence, each fluorescence spectroscopy of BSA in the presence of different RA concentration was corrected using the following equation[21,22]:

$$F_{cor} = F_{obs} e^{(A_{ex} + A_{em})/2} \quad (1)$$

where F_{cor} and F_{obs} are the fluorescence intensities corrected and observed, respectively; and A_{ex} and A_{em} are the absorption of the system at the excitation and emission wavelengths, respectively. The fluorescence intensity utilized in this paper was the corrected fluorescence intensity.

Fluorescence quenching of BSA by RA

Fluorescence spectroscopy is a powerful and very sensitive technique, which can be

used to investigate the interaction between proteins and ligands[21]. Protein fluorescence is mostly excited at the absorption maximum near 280 nm or at longer wavelengths. The absorption of proteins at 280 nm is due to both Tyr and Trp residues, whereas at wavelength longer that 295 nm, the absorption is primarily due to Trp[22].

The *in vitro* fluorescence quenching measurement of BSA in the absence and presence of RA was carried out and the binding was fully characterized. Fig. 2A displayed that the effect of RA on BSA fluorescence intensity upon excitation at 280 nm at 298 K. It can be seen that there was no fluorescence emission for RA (curve *0*) at the range measured. The fluorescence intensity of BSA at peak 345 nm decreased regularly with the concentration of RA increasing from 0 to 6×10^{-5} mol L^{-1}, and the maximum emission wavelength had occurred a red shift, which implying that RA could interact with BSA, and the microenvironment around the chromophore of BSA was changed after adding RA[25].

In order to determine whether Tyr and/or Trp residues were involved in the interaction with the RA, the fluorescence of BSA excited at 280 and 295 nm were compared. The plots of F/F_0 against [RA]/[BSA] were presented in Fig. S1 (ESI†). As found in Fig. S1 (ESI†), no apparent difference can be seen for the extension of BSA fluorescence quenching when excited at 280 and 295 nm. This phenomenon showed that only the Trp residue was implicated in the fluorescence quenching and that Try residue did not take part in the binding reaction between BSA and RA[26]. It also illustrated that the binding site for RA on BSA was in the vicinity of Trp residue[26].

The mechanism of observed fluorescence quenching could be due to either static or dynamic mechanism or a combination of both these processes[27]. To confirm the type of fluorescence quenching mode, the fluorescence quenching data of BSA was analyzed by the well-known Stern-Volmer equation[28,29]:

$$\frac{F_0}{F} = 1 + K_{SV}[Q] = 1 + k_q \tau_0 [Q] \quad (2)$$

where F_0 and F are the fluorescence intensities in the absence and presence of RA, respectively. K_{SV} is the Stern–Volmer quenching constant for protein; [Q] is the concentration of quencher; k_q is the quenching rate constant of the biological macromolecule; τ_0 stands for the fluorescence lifetime in the absence of quencher and its value for BSA is 10^{-8} s. The Stern-Volmer curves of F_0/F versus [Q] at the excitation wavelengths of 280 nm in the BSA-RA system were plotted in Fig. 2B. The observed apparent deviation from linearity of the Stern-Volmer plots (upward curvature) usually represented the signature of the quenching mechanism being governed by the simultaneous operation of both static and dynamic quenching and/or high extent of quenching in the higher concentration regime of the quencher. However, a linear Stern-Volmer plot in nature indicated that the fluorescence quenching type was either the static or the dynamic quenching[30]. In this paper, to provide a semiempirical measure of the magnitude of the quenching in all research systems, the quenching in terms of K_{SV} and k_q values at low quencher concentrations where the plots are nearly linear was investigated (Fig. 2B). The good fitting linearity with R-square > 0.99 (Table 1) suggested that the Stern-Volmer model was appropriate for studying the binding mechanism between BSA and RA. The results in Table 1 showed the K_{SV} was inversely correlated with temperature, indicating that the probable quenching mechanism of BSA-RA binding reaction was static. Moreover, the k_q values, calculated by K_{SV}/τ_0, had an order of magnitude of 10^{12}, which were much greater than 2.0×10^{10} L mol^{-1} s^{-1}, the maximum diffusion collision quenching rate constant for a biomacromolecule dissolved in water[31]. Thus, we can conclude that the quenching process was predominantly static, that is, the quenching might be chiefly initiated by a ground-state complex formation. Consequently, a conclusion

could be safely drawn that the dynamic quenching was not the dominant quenching mechanism, at least at low RA concentrations, and that the interaction of RA with BSA was characteristic of the combined quenching mechanism.

For a static quenching procedure, the data were investigated based on the modified Stern-Volmer equation[32,33]:

$$\frac{F_0}{F_0 - F} = \frac{1}{f_a} + \frac{1}{f_a [Q] K_a} \quad (3)$$

where f_a is the fraction of accessible fluorescence, and K_a is the effective quenching constant for the accessible fluorophores, which are analogous to associative binding constants for the quencher-acceptor system. Table 1 summarized the values of K_a at three temperatures. The decreasing trend of K_a with the increasing temperature was consistent with dependence of K_{SV} on the temperature. This therefore further indicated that the fluorescence quenching of BSA was a static quenching mechanism.

Fig. 2

Table 1

Binding constant and the number of binding sites

Results from fluorescence measurements can be utilized to calculate the binding constant K and the stoichiometry of binding n of the complex using the Scatchard equation[34,35]:

$$r / D_f = nK - rK \quad (4)$$

where r is the moles of ligand bound per mole of protein, D_f is the molar concentration of free ligand, n is the number of binding sites per BSA molecule, and K denotes the equilibrium binding constant. The plot of r/D_f versus r was displayed in Fig. 2C and the values of K and n were summarized in Table 2. The linearity of the

Sactchard plots indicated that RA bound to a class of binding site on BSA, which was full in agreement with the number of the binding site *n* (approximately equal to 1)[35,36]. It can be seen from the Table 2 that the binding constants were all in the order of magnitude larger than 10^4 L mol^{-1}. This result was in agreement with many earlier papers[32,33], and such value of *K* illustrated that the binding affinity between BSA and RA was moderate, and it can be considered to be good for RA to diffuse from vascular system to its target sites[32,33]. Moreover, the binding constants for BSA-RA system decreased with the temperature rose, specifying that the protein-ligand binding strength was getting weak[36].

To further verify how many molecules of RA can be bound by BSA, the Job's plot analysis (known as the method of continuous variation) was carried out. Job's plot is a very useful method for the characterization of the complex formed by an interaction of two species[37]. It was performed by preparing 11 solutions covering the whole range of molar fractions of RA and BSA, while maintaining the total concentration ([BSA]+[RA]) constant. A plot of the molar fraction of RA versus the difference in fluorescence intensity ($\Delta F = F_{BSA}$-F_{BSA+RA}) was then made. Finally, a special point was obtained from the plot and the binding stoichiometry was calculated from the molar fraction of RA at that specific point. As was evident from the Job's plot (the specific point located in 0.5), implied that the stoichiometric ratio of BSA: RA at 298 K was 1:1 (Fig. 2D)[38].

Table 2

Thermodynamic parameters and binding forces

The knowledge of the actual binding forces governing the protein-ligand interaction process is of primary importance in the context of the research in this field, and it can be learned from the thermodynamic parameters. In general, there exist four types of

non-covalent interaction forces in the binding of small molecular substance of protein: hydrogen bonds, van der Waals forces, hydrophobic and electrostatic interactions[7]. The signs and magnitudes of thermodynamic parameters for the protein-ligand binding reaction have often been invoked to provide a simple way to account for the principal binding forces. The standard enthalpy change ΔH^0 can be considered as a constant when the temperature changes in a small scope, then the thermodynamic parameters (standard enthalpy change (ΔH^0), standard entropy change (ΔS^0) and free energy change (ΔG^0) can be calculated from Van't Hoff equation[39]:

$$\log K = \frac{-\Delta H^0}{2.303RT} + \frac{\Delta S^0}{2.303R} \quad (5)$$

$$\Delta G^0 = \Delta H^0 - T\Delta S^0 \quad (6)$$

where K is the binding constant and R is the universal gas constant. ΔH^0 and ΔS^0 were obtained from the plot of log$K$ versus $1/T$ (Fig. 3A), and the calculated thermodynamic parameters at 288, 298, 308 K were summarized in Table 2. As shown is Table 2, the negative ΔG^0, negative ΔH^0 and positive ΔS^0 revealed that the interaction between BSA and RA was enthalpically as well as entropically favored, and a spontaneous binding process[26]. According to the rules summarized by Ross and Subramanian[40], the different sign and magnitude for thermodynamic parameters were associated with various kinds of interaction forces. In general, form the point view of water structure, a positive ΔS^0 value is frequently taken as typical evidence for hydrophobic interaction. Moreover, the negative ΔH^0 value of BSA-RA system cannot be mainly attributed to electrostatic interaction since the ΔH^0 of electrostatic interaction is very small, almost zero. A negative value is observed whenever there is hydrogen bonding in the binding. Therefore, it was more likely that both hydrophobic and hydrogen bond interactions played an important role in the BSA-RA binding

reaction. In addition, from Table 2, K decreased with the increase of temperature, because the ΔH^0 was negative and the binding process was an exothermic reaction.

Identification of the binding sites of RA on BSA

From different investigations, it has been suggested that BSA has limited number of binding sites. In the light of site marker displacement method, it has been detected that there exist at least three relatively high affinity binding sites on BSA[33]. These sites are commonly called the warfarin, the ibuprofen and the digitoxin binding sites which are also called as site I, site II and site III, respectively. In this paper, site marker competitive experiments have been carried out using warfarin, ibuprofen and digitoxin that specifically bind to BSA binding site I, II and III, respectively. Firstly, increasing amounts of site markers were added to a mixture containing fixed concentrations of BSA-RA complex, here it should be noted that the ratio of RA to BSA was kept at 4:1 to maintain the nonspecific binding of probes to a minimum. And then the fluorescence emission spectra were recorded with an excitation wavelength of 280 nm. Finally, the percentage of the specific site bound by RA was obtained by measuring the changes in fluorescence intensity[41]:

$$Probe\ displacement\ (\%) = \frac{F_2}{F_1} \times 100\% \quad (7)$$

where F_1 and F_2 are the fluorescence of BSA-RA in the absence and presence of the site marker, respectively. The plot of *Probe displacement* (%) against the concentration ratio of site marker to BSA were shown in Fig. 3B. It can be seen from Fig. 3B that the fluorescence intensity of BSA-RA was influenced by the addition of warfarin, while for ibuprofen and digitoxin it remained fairly constant. The results indicated that the bound RA to BSA was obviously affected by adding warfarin. Hence, RA was most likely bound to the hydrophobic pocket located within site I

(subdomain IIA) of BSA[42].

Energy transfer from BSA to RA

Fluorescence resonance energy transfer (FRET) is a distance-dependent interaction between the electronic excited states of two molecules in which excitation is transferred from a donor molecule to an acceptor molecule without emission of a photon[39]. The efficiency of FRET is dependent on the inverse sixth power of the intermolecular separation, making it useful over distances comparable to the dimensions of biological macromolecules. Thus, FRET is an important technique for investigating a variety of biological phenomena that produce changes in molecular proximity. According to Förster's non–radiation energy transfer theory[43], the distances between the protein residue (donor) and the bound ligand (acceptor) in BSA could be obtained. The efficiency of energy transfer between the donor (BSA) and acceptor (RA), E, could be calculated by the following equation[7]:

$$E = 1 - \frac{F}{F_0} = \frac{R_0^6}{R_0^6 + r^6} \tag{8}$$

where r is the mean distance between the centers of the donor and acceptor dipoles; R_0 is the critical distance when the transfer efficiency is 50% and it can be calculated from donor emission and acceptor absorption spectra by using the Förster's formula[7]:

$$R_0^6 = 8.79 \times 10^{-25} K^2 N^{-4} \Phi J \tag{9}$$

where K^2 is the spatial orientation factor of the dipole ($K^2 = 2/3$); N is the average refractive index of medium; Φ is the fluorescence quantum yield of the donor; J is the overlap integral of the fluorescence emission spectrum of the donor and the absorption spectrum of the acceptor. It is given by[7]:

$$J = \frac{\sum F(\lambda)\varepsilon(\lambda)\lambda^4 \Delta\lambda}{\sum F(\lambda)\Delta\lambda} \tag{10}$$

where $F(\lambda)$ is the fluorescence intensity of the donor at the wavelength λ, $\varepsilon(\lambda)$ is the

molar absorption coefficient of the acceptor when the wavelength is λ. The overlap of the fluorescence emission spectrum of BSA and the absorption spectrum of RA at 298 K was displayed in Fig. 3C. Hence, the overlap integral was calculated to be $J = 1.018 \times 10^{-14}$ cm^3 L mol^{-1} by integrating the spectra for 300-500 nm. In the BSA-RA system, $K^2 = 2/3$, $N = 1.36$, $\Phi = 0.15$[44]. According to these parameters, we could obtain that $R_0 = 2.529$ nm, $E = 0.222$ and $r = 3.118$ nm. Obviously, the values for (r) and (R_0) were within 8 nm and $0.5R_0 < r < 1.5R_0$, suggesting that the energy transfer between BSA and RA can occur with high possibility. The results indicated again a static quenching between BSA and RA because of the formation of BSA-RA complex.

Fig. 3

Time-resolved measurements

Time-resolved fluorescence spectroscopy is used to monitor molecular interactions and motions that occur in the picosecond-nanosecond time range, and is especially useful in the analysis of biomolecular structure and dynamics[45]. From time-resolved fluorescence measurements, the fluorescence lifetime can be determined. The fluorescence lifetime can be used to characterize a fluorescent molecule. It is, however, also influenced by the chemical composition of its environment. Lifetime changes can therefore be used to gain information about the local chemical environment or to follow reaction mechanisms. Fig. 4A displayed the typical lifetime decays of BSA in the absence and presence of RA. The lifetime decays for all the measurements were found to be biexponential having very good χ^2 values and the relevant decay parameters were summarized in Table 3. The average lifetimes $\langle\tau\rangle$ were calculated from the following equation[46]:

$$\langle\tau\rangle = \frac{A_1\tau_1 + A_2\tau_2}{A_1 + A_2} \quad (11)$$

where A_1, A_2 and τ_1, τ_2 are the relative amplitudes and the corresponding decay time constants of the individual components in biexponential decay profiles, respectively. In the absence of RA, BSA exhibited a biexponential decay curve with an average lifetime $<\tau>$ of 6.186 ns and having lifetime components of 5.403 ns and 7.320 ns with the relative abundance of 49.8% and 50.2%, respectively. A similar kind of biexponential fluorescence decay of BSA can be found in earlier literature and assigned to the presence of two tryptophan residues at different conformational states in two distinct chemical environments[21]. It was important to note that the average lifetime of BSA progressively reduced with the increase of the RA concentration, which illustrated that the microenvironment of tryptophan residues was changed and the complex between BSA and RA formed[21]. It also attested that the quenching mechanism was not governed by the only static quenching mechanism but the simultaneous operation of both static and dynamic quenching or the only dynamic quenching, because for static quenching the fluorescence lifetime will not change significantly[21]. To further delve into the quenching mechanism, we investigated the ratio of the static quenching in the whole quenching process. The time-resolved Stern-Volmer plot ($<\tau_0>/<\tau>$ vs. [RA]) and compared with the corresponding Stern-Volmer curve (F_0/F vs. [RA]) were shown in Fig. 4B. It was observed that the time-resolved Stern-Volmer plot was below the Stern-Volmer curve, which suggested that there was a static quenching in the fluorescence quenching procedure. The ratio of excited species that were quenched statically (f_{static}) can be calculated from $f_{static} = 1-((<\tau_0>/<\tau>)/(F_0/F))$[46]. Thus, for BSA-RA system f_{static} was 84.28%, that is, the static quenching in the intrinsic fluorescence of BSA accounted for 84.28% of the whole quenching procedure, which demonstrated that the static quenching was the dominant quenching mechanism. Consequently, both static and dynamic quenching were

involved in the binding process, but the static quenching mechanism was the dominant one.

Fig. 4

Table 3

Conformational studies

Here, conformational changes occurring in the BSA on binding were investigation by using UV-vis absorption, synchronous fluorescence, three-dimensional fluorescence, ANS fluorescence, FT-IR, CD and NMR methods.

UV-vis absorption spectra

UV–vis absorption spectroscopy is a reliable tool to understand the morphological changes in secondary structure of protein and to investigate protein-ligand complex formation. Fig. S2 (ESI†) shown the effect of RA on the BSA absorption spectra. In BSA, the strong absorption peak (about 210 nm) represented the α-helical structure of BSA, while the weak absorption peak at 280 nm arisen from the phenyl rings in aromatic amino acids[21]. It can be seen from Fig. S1 (ESI†), the intensity of the peak at 210 nm reduced with a red-shift upon adding the RA. The results clearly illustrated that the conformation of BSA was changed and RA bound to BSA. That is to say, a new complex between BSA and RA formed.

Synchronous fluorescence spectroscopy

Synchronous fluorescence spectroscopy introduced by Lloyd[47] can be applied to infer the conformational changes of the protein and analyze the interaction between small compounds and proteins. It is possible to measure the shift in maximum emission wavelength, corresponding to the change in polarity around the chromophore molecule. When the scanning interval value ($\Delta\lambda$) between the excitation and emission wavelength is maintained at 15 and 60 nm, the synchronous fluorescence gives

spectral behaviors of tyrosine and tryptophan residues of BSA, respectively[41,44]. The synchronous fluorescence spectra of BSA with adding different concentrations of RA was shown in Fig. S3 (ESI†). It can be seen from Fig. S3 (ESI†), the maximum wavelength of tyrosine residue kept basically unchanged, whereas a slight red shift can be found when $\Delta\lambda$ = 60 nm, indicating the microenvironment around tyrosine residue had no discernable change, and the polarity around tryptophan residue increased and the hydrophobicity decreased.

Three-dimensional fluorescence spectroscopy

The three-dimensional fluorescence spectroscopy is a newly developed fluorescence analytical technique and has become more and more popular in recent years. It can extensively reflect the fluorescence information of the protein, making investigation of the characteristic conformational change of BSA more scientific and credible[44]. The three-dimensional fluorescence spectra and the corresponding contour maps of BSA and BSA-RA system were exhibited in Fig. S4 (ESI†), and the related characteristic parameters were listed in Table 4. As shown in Fig. S4 (ESI†), Peak a is the Rayleigh scattering peak ($\lambda_{em} = \lambda_{ex}$), and Peak b is the second-order scattering peak ($\lambda_{em} = 2\lambda_{ex}$). Because when λ_{ex} = 280 nm, the emission spectra can mainly display the intrinsic fluorescence of tryptophan and tyrosine residues, as the main fluorescence peak, Peak 1 primarily shows the spectral behavior of tryptophan and tyrosine residues. Besides Peak 1, there is another fluorescence peak 2, which chiefly exhibits the fluorescence spectral behavior of BSA's characteristic polypeptide backbone structure, that caused by the $P \rightarrow P^*$ transition of structure C=O of BSA[48]. From Table 4, we can find that the addition of RA induced a significant decrease in the intensity along with a red shift in both Peak 1 and 2. The phenomenon allowed us to conclude that the interaction between RA and BSA resulted in a slight unfolding of the

polypeptides of BSA, which induced a conformational changes. All in all, the above research findings disclosed some conformational and microenvironmental change of BSA caused by the binding of RA.

Table 4

ANS fluorescence spectroscopy

The intrinsic fluorescence spectroscopy only indicates the structural change around aromatic amino acids motifs, so more studies should be carried out to make a systematic investigation of the conformational change of BSA induced by the binding of RA. ANS, as a fluorescent molecular probe, can be used to study conformational changes induced by ligand binding in proteins, as ANS's fluorescent properties will change as it binds to hydrophobic regions on the protein surface[26,49]. Comparison of the fluorescence in the presence and absence of a particular ligand can thus give information about how the binding of the ligand changes the surface of the protein. To obtain more information on the binding of RA to BSA, the ANS fluorescence spectroscopy was carried out and the results were shown in Fig. 5A. RA alone or RA incubated with ANS had negligible fluorescence intensities, suggesting that there was no interaction between RA and ANS. In contrast, the fluorescence intensity of ANS-BSA system decreased with the addition of RA, but no significant shift in fluorescence emission peak was observed. These findings illustrated that RA could reduce the hydrophobic surface of BSA which made the ANS fluorescence quenching.

FT-IR spectra measurement

FT-IR has emerged as an efficient tool for the characterization of the drug-protein interaction. The IR spectrum of a protein exhibits a number of amide bands that represent different vibrations of the peptide moiety[50]. For the protein, nine

characteristic vibrational bands or group frequencies have been identified, namely, amide A, B and I-VII. Of these, the amide I band (1600-1700 cm^{-1}, mainly C=O stretch) and amide II band (1500-1600 cm^{-1}, C-N stretch coupled with N-H bending mode) are the two most prominent vibrational bands of the protein backbone, and they both have a relationship with the secondary structure of the protein[51]. Fig. 5B showed the FT-IR spectra of free BSA and the difference spectra of BSA (subtracting the absorption of the RA-free form from that of the BSA-RA bound form). It clearly showed that the peak position of amide I band was shifted from 1659.47 to 1666.93 cm^{-1}, while that of amide II band was moved to a lesser extent from 1548.50 to 1543.87 cm^{-1}. The changes of these peak positions and peak shapes illustrated that RA interacted with BSA and caused a change in the secondary structure of BSA. The drug interacted with C=O and C-N groups in protein and resulted in rearrangement of polypeptide carbonyl hydrogen bonding network.

Fig. 5

CD spectra analysis

Circular dichroism method (CD) can be used in protein studies to look at characterization, stability, formulation, structure and more. CD spectroscopy is a powerful technique particularly suited to prove the specific binding of small compounds to chiral macromolecules, and also to detect sensitive structure changes of protein caused by ligands[52,53]. In general, CD spectra of proteins can be divided into two wavelength regions. The far-UV CD spectrum of proteins can reveal important characteristics of their secondary structure, but the near-UV CD spectrum can provide information on the tertiary structure[54]. Fig. 6A showed the far-UV CD spectra of BSA in the absence and presence of the RA at room temperature. There were two negative humped peaks at 208 nm and 220 nm, which represented the transition of π-π* and

572 n-π* of α-helix peptide bond, respectively, and also were characteristic of the typical
573 α-helix structure of protein[41,53]. It can be seen from Fig. 6A that the addition of RA
574 caused the CD signal of BSA to decrease without any significant shift of the band,
575 indicating that there were some loss in the α-helix structure and the secondary
576 structure of protein had changed. This might arise from the formation of the BSA-RA
577 complex. Moreover, the shape of the CD spectra of BSA had no obvious changed in
578 the presence of RA, suggesting that the structure of BSA was still predominantly
579 α-helix even after binding to RA. Due to the structure of BSA was mainly α-helical,
580 so in this paper we considered primarily the changes in α-helical contents of BSA.
581 Generally, the CD results were expressed in terms of mean residue ellipticity (MRE)
582 in deg cm^2 dmol^{-1} according to the following equation[55]:

583 $$\mathrm{MRE} = \frac{observed\ CD\ (m\deg)}{C_P \times n \times l \times 10} \quad (12)$$

584 where n is the number of amino acid residues (n = 583 for BSA); C_p is the
585 concentration of BSA in mol L^{-1}; l is the path length. The content of α–helix in free
586 and complexed BSA can be calculated from MRE values at 208 nm using the
587 following equation[7,41,55]:

588 $$\alpha\text{-helix}(\%) = \frac{-\mathrm{MRE}_{208} - 4000}{33000 - 4000} \times 100 \quad (13)$$

589 where MRE_{208} is the experimental MRE value at 208 nm. Compared with the free
590 BSA, it was obvious that the α–helix content of BSA was decreased from 53.80% to
591 50.62% at a molar ratio of BSA to RA of 1:12. It can be obtained that the secondary
592 structure of BSA had changed during the reaction between BSA and RA. This result
593 also indicated that RA bound with the amino acid residue of the main polypeptide
594 chain of BSA, and wrecked their hydrogen bonding networks. These observations
595 were also consistent with above FT-IR experimental results.

On the other hand, the changes in the tertiary structure were studied by monitoring the near-UV CD spectra (260 to 320 nm) of the protein in the absence and presence of RA. Unlike in far-UV CD, the near-UV CD spectrum cannot be assigned to any particular three-dimensional structure. The signals obtained in the 260-320 nm region are due to the absorption, dipole orientation and the nature of the surrounding environment of the phenylalanine, tyrosine, tryptophan and cysteine (or S-S disulfide bridges) amino acids[56]. As was depicted in Fig. 6B, BSA showed two minima at 262 and 268 nm and a shoulders around 290 nm. Increasing the RA concentration caused a regular decrease in the ellipticity at 262 and 268 nm and an apparent increase around 290 nm. These changes suggested the perturbations around disulfide bridges and aromatic chromophores of BSA upon complexation with RA, namely the occurrence of tertiary structural alteration of BSA.

Fig. 6

NMR analysis for BSA-RA system

Nuclear magnetic resonance (NMR) technique has evolved into a powerful tool for characterizing protein–ligand interactions, particularly for screening applications in the pharmaceutical industry, in solution under near physiological conditions[57]. In the study of weak low-affinity protein-ligand interaction, NMR parameters of drug molecule, such as chemical shift, relaxation time and self-diffusion coefficient can be detected. Although the current resolution of one-dimensional NMR spectra is not high enough to locate the protons of BSA due to the complicated structure of BSA, the ^{1}H NMR signal changes of RA with and without BSA are investigated to monitor their interactions[57]. In this study, the concentration RA of was fixed and the concentration of BSA was gradually increased. Fig. 7 shown the ^{1}H NMR spectra of RA in the absence and presence of BSA. It can be seen that the resolution loss of proton signals

621 of RA was monitored and its loss extent was enhanced with the increased BSA
622 concentration. When the concentration of BSA was 2.5×10^{-4} mol L^{-1}, the broadened
623 effect may be attributed to the external viscosity of protein solution[58]. Instead, when
624 the molar ratio of RA/BSA was 100:1, the proton signals were broadened and the split
625 peaks arising from spin-spin coupling overlapped into one. It can be concluded that
626 RA combined with BSA and the alteration of effective field at the protons of RA
627 caused by the interaction between RA and BSA. Moreover, the ^{1}H signals of aromatic
628 section shifted downfield when adding BSA, which was due to the magnetic
629 deshielding effects in the complex formation with BSA, mainly contributed by the
630 hydrogen bonds[59,60]. After all, the results above indicated that there existed apparent
631 interaction between BSA and RA.

632 Fig. 7

633 **Molecular docking studies**

634 Molecular docking is assuming an increasingly significant method in realizing the
635 foundation of ligand-protein recognitions. According to the site marker competitive
636 experiments, we found that RA bound to site I (subdomain IIA) of BSA. To explain
637 the recognition mode between RA and BSA more fully, molecular docking was
638 conducted, and the best docking energy results were shown in Fig. 8A. The docking
639 results indicated that RA was located at the binding pocket of subdomain IIA (Fig.
640 8C). Furthermore, RA was adjacent to some hydrophobic residues in subdomain IIA
641 of BSA (Leu-209, Val-239, Leu-196, Trp-212, Ala-289 and Leu-236), suggesting that
642 the presence of hydrophobic interactions between RA and BSA (Fig. 8B). Moreover,
643 two hydrogen bonds were found between the hydroxyl group of RA and Glu-151
644 residue, Arg-197 residue; the hydrogen bond lengths, respectively, were 2.56 Å and
645 2.87 Å. And Arg-216 residue was in suitable position to form a hydrogen bond with

carboxyl group of RA with distance of 2.83 Å. In addition, RA also had potential π-interactions with some residues (Arg-255, Arg-197, His-240, Trp-212 and Arg-216). On the basis of the molecular docking described above, we came to the conclusion that the RA was situated within site I, and the main driving forces were hydrophobic interactions and hydrogen bonds, which were in agreement with the fluorescence data. It was also important to note that the Trp-212 residue of BSA was in close neighborhood to the RA, which provided a reliable structural foundation to illustrate the efficient fluorescence quenching of BSA emission in the presence of RA.

Fig. 8

Molecular dynamics simulations

To evaluate the structural stability of the BSA-RA system, the properties were examined by means of the root mean square deviation (RMSD) and root mean square fluctuation (RMSF) of the protein. As shown in Fig. 9A, the RMSD values of atoms in the unliganded BSA and BSA-RA complex were plotted from 0 to 11 ns. The analysis of RMSD indicated both systems (BSA and BSA-RA complex) reached stability and balance after 3.5 ns simulation time till the end of the MD simulation, 11 ns, indicating that the molecular systems were well behaved thereafter. The calculated average RMSD values of BSA and BSA-RA complex were 2.05 ± 0.20 nm and 2.44 ± 0.15 nm, respectively, when they achieved an equilibrium state. In addition, the RMSF of all amino acid residues of BSA in the RA was examined to reveal the flexibility of residues of BSA. Fig. 9B described the plot of RMSF against residue number. The results indicated that all of the residues in the RA binding site (Ala-141 – Glu-151, Glu-185 – Lys-220 and Leu-236 – Gly-246) had relative small degree of flexibility, illustrating that residues locating in the drug binding site (site I) seem to be more rigid due to the BSA-RA complex formation. In brief, the fluctuations of the

residues at the binding site clearly certified that RA specifically bound to the site I in BSA.

Fig. 9

Conclusions

In summary, this study described a spectral deciphering of the interaction of RA with a model transport protein BSA under physiological conditions, which were dissected by blending with UV-vis absorption, fluorescence, FT-IR, CD, NMR spectra and molecular modeling. Analysis of fluorescence data of BSA showed that RA effectively quenched the fluorescence of BSA primarily through static quenching mechanism, but in the binding process the dynamic quenching can't be ignored. The binding constant of BSA-RA complex was calculated to be 4.18×10^4 L mol^{-1} at 298 K, and the average binding distance (r) between BSA and RA was estimated to be 3.118 nm according to the Förster's theory of non–radiation energy transfer theory. The results explained that RA was found to spontaneously fasten in subdomain IIA, Sudlow's site I of BSA, substantially by the noncovalent interactions such as hydrophobic interactions and hydrogen bonds. Additionally, the binding of RA to BSA induced small conformational and micro-environmental changes in the structure of BSA, proved by the research data of the UV–vis absorption, synchronous fluorescence, three-dimensional fluorescence, ANS fluorescence, FT-IR spectroscopy, and CD spectra experiments. NMR data further confirmed that RA can bind to BSA, and the aromatic groups of RA played an essential role during the binding reaction. These results were also well supported by the molecular modeling study. No doubt, all these results are important to comprehensively understand the distribution and metabolism of RA *in vivo*, which could be a useful guideline for clarifying dynamic of RA. Furthermore, the investigation of interaction can provide vital insight into

functional substance screening at the early stage of health foods research.

Funding

This work was supported by the Natural Science Foundation of China (Nos. 21476165, 51173128, 21306134), the 863 Program of China (No. 2013AA102204), the Ministry of Science and Technology of China (No. 2012YQ090194), the Ministry of Education (No. 20130032120029), the Beiyang Young Scholar of Tianjin University (2012) and the Program of Introducing Talents of Discipline to Universities of China (No. B06006).

Notes

The authors declare no competing financial interest.

Abbreviations

ANS	8-anilino-1-naphthalenesulfonic acid
Ala	Alanine
Arg	Arginine
BSA	Bovine serum albumin
CD	Circular dichroism
FRET	Fluorescence resonance energy transfer
FT-IR	Fourier transform infrared spectroscopy
Glu	Glutamic acid
Gly	Glycine
His	Histidine
HSA	Human serum albumin
Leu	Leucine
Lys	Lysine

MD	Molecular dynamic
MRE	Mean Residue Ellipticity
NMR	Nuclear magnetic resonance
RA	Rosmarinic acid
RMSD	Root mean square deviation
RMSF	Root mean square fluctuation
Trp	Tryptophan
Tyr	Tyrosine
UV-vis	Ultraviolet-visible spectroscopy
Val	Valine

Acknowledgements

We thank the Chemical Engineering Research Center, Tianjin University, for providing all the necessary facilities to carry out this work. Thanks also go to the reviewers of this manuscript for their priceless and constructive suggestions.

References

1 A. Crozier, I. B. Jaganath and M. N. Clifford, *Nat. Prod. Rep.*, 2009, **26**, 1001-1043.

2 M. Petersen, *Phytochem. Rev.*, 2013, **12**, 207-227.

3 Y. Zhang, X. Q. Chen, L. Yang, Y. G. Zu and Q. Lu, *Food Funct.*, 2015, **6**, 927-931.

4 F. Zhu, T. Asada, A. Sato, Y. Koi, H. Nishiwaki and H. Tamura, *J. Agric. Food Chem.*, 2014, **62**, 885-892.

5 S. Baba, N. Osakabe, M. Natsume, A. Yasuda, Y. Muto, T. Hiyoshi, H. Takano, T. Yoshikawa and J. Terao, *Eur. J. Nutr.*, 2005, **44**, 1-9.

6 T. Nakazawa and K. Ohsawa, *J. Nat. Prod.*, 1998, **61**, 993-996.

7 X. Pan, P. Qin, R. Liu and J. Wang, *J. Agric. Food Chem.*, 2011, **59**, 6650-6656.

8 Z. Chi, R. Liu, Y. Teng, X. Fang and C. Gao, *J. Agric. Food Chem.*, 2010, **58**, 10262-10269.

9 Y. Yang, X. Yu, W. Tong, S. Lu, H. Liu, Q. Yao and H. Zhou, *J. Solution Chem.*, 2013, **42**,

666-675.

10 X. Zhang, L. Li, Z. Xu, Z. Liang, J. Su, J. Huang and B. Li, *Plos One*, 2013, **8**, e59106.

11 L. M. Berezhkovskiy, *J. Pharm. Sci.*, 2007, **96**, 249-257.

12 J. Xiao, M. Wu, G. Kai, F. Wang, H. Cao and X. Yu, *Nanomed-Nanotechnol.*, 2011, **7**, 850-858.

13 A. Papadopoulou, R. J. Green and R. A. Frazier, *J. Agric. Food Chem.*, 2005, **53**, 158-163.

14 G. W. Zhang and Y. D. Ma, *Food Chem.*, 2013, **136**, 442-449.

15 J. Tang, G. Liang, C. Zheng and N. Lian, *J. Solution Chem.*, 2013, **42**, 226-238.

16 M. Skrt, E. Benedik, Č. Podlipnik and N. P. Ulrih, *Food Chem.*, 2012, **135**, 2418-2424.

17 L. Trnková, I. Boušová, V. Kubíček and J. Držata, *Nat. Sci.*, 2010, **2**, 563-570.

18 G. S. Wu, D. H. Robertson, C. L. Brooks and M. Vieth, *J. Comput. Chem.*, 2003, **24**, 1549-1562.

19 W. L. Jorgensen, J. Chandrasekhar, J. D. Madura, R. W. Impey and M. L. Klein, *J. Chem. Phys.*, 1983, **79**, 926-935.

20 T. Darden, D. York and L. Pedersen, *J. Chem. Phys.*, 1993, **98**, 10089-10092.

21 Z. Chi and R. Liu, *Biomacromolecules*, 2010, **12**, 203-209.

22 X. Zhao, R. Liu, Z. Chi, Y. Teng and P. Qin, *J. Phys. Chem. B*, 2010, **114**, 5625-5631.

23 B. K. Paul, D. Ray and N. Guchhait, *Phys. Chem. Chem. Phys.*, 2013, **15**, 1275-1287.

24 X. Guo, L. Zhang, X. Sun, X. Han, C. Guo and P. Kang, *J. Mol. Struct.*, 2009, **928**, 114-120.

25 J. Toneatto and G. A. Argüello, *J. Inorg. Biochem.*, 2011, **105**, 645-651.

26 X. Peng, Y. H. Sun, W. Qi, R. X. Su and Z. M. He, *J. Solution Chem.*, 2014, **43**, 585-607.

27 X. Li, G. Wang, D. Chen and Y. Lu, *Mol. BioSyst.*, 2014, **10**, 326-337.

28 J. R. Lackowicz, *Principles of fluorescence spectroscopy*, 3rd edn, Plenum Press, New York, 2006, pp. 63-606.

29 S. Soares, N. Mateus and V. De Freitas, *J. Agric. Food Chem.*, 2007, **55**, 6726-6735.

30 B. K. Paul, N. Ghosh and S. Mukherjee, *Langmuir*, 2014, **30**, 5921-5929.

31 S. M. Darwish, M. M. Abu Teir, S. A. Makharza and M. M. Abu-hadid, *J. Mol. Struct.*, 2010, **963**, 122-129.

32 Y. J. Hu, Y. Liu and X. H. Xiao, *Biomacromolecules*, 2009, **10**, 517-521.

33 J. Q. Tong, F. F. Tian, Q. Li, L. L. Li, C. Xiang, Y. Liu, J. Dai and F. L. Jiang, *Photoch. Photobio. Sci.*, 2012, **11**, 1868-1879.

34 G. Scatchard, *Ann. NY. Acad. Sci.*, 1949, **51**, 660-672.

35 X. Wang, X. Xie, C. Ren, Y. Yang, X. Xu and X. Chen, *Food Chem.*, 2011, **127**, 705-710.

36 X. Xie, Z. Wang, X. Zhou, X. Wang and X. Chen, *J. Hazard. Mater.*, 2011, **192**, 1291-1298.

37 C. Y. Huang, *Method. Enzymol.*, 1982, **87**, 509-525.

38 F. Ding, W. Liu, J. X. Diao and Y. Sun, *J. Hazard. Mater.*, 2011, **186**, 352-359.

39 S. N. Khan, B. Islam, R. Yennamalli, A. Sultan, N. Subbarao and A. U. Khan, *Eu. J. Pharm. Sci.*, 2008, **35**, 371-382.

40 P. D. Ross and S. Subramanian, *Biochemistry-US*, 1981, **20**, 3096-3102.

41 N. Ibrahim, H. Ibrahim, S. Kim, J. P. Nallet and F. Nepveu, *Biomacromolecules*, 2010, **11**, 3341-3351.

42 T. Xu, X. Guo, L. Zhang, F. Pan, J. Lv, Y. Zhang and H. Jin, *Food Chem. Toxicol.*, 2012, **50**, 2540-2546.

43 T. Förster and O. Sinanoglu, *Modern quantum chemistry*, Academic Press, New York, 1965, pp. 93-137.

44 Y. Liu, M. Chen, Z. Luo, J. Lin and L. Song, *J. Biomol. Struct. Dyn.*, 2013, **31**, 1160-1174.

45 W. Peng, F. Ding, Y. Jiang, Y. Sun and Y. Peng, *Food Funct.*, 2014, **5**, 1203-1217.

46 J. Ma, Y. Liu, L. Chen, Y. Xie, L. Y. Wang and M. X. Xie, *Food Chem.*, 2012, **132**, 663-670.

47 J. B. F. Lloyd and I. W. Evett, *Anal. Chem.*, 1977, **49**, 1710-1715.

48 S. R. Feroz, S. B. Mohamad, N. Bujang, S. N. A. Malek and S. Tayyab, *J. Agric. Food Chem.*, 2012, **60**, 5899-5908.

49 M. Liu, W. Zhang, L. Qiu and X. Lin, *J. Biochem.*, 2011, **149**, 27-33.

50 Y. Li, H. Wang, B. Jia, C. Liu, K. Liu, Y. Qi and Z. Hu, *Food Addit. Contam. A*, 2013, **30**, 356-364.

51 B. Hemmateenejad, M. Shamsipur, F. Samari, T. Khayamian, M. Ebrahimi and Z. Rezaei, *J. Pharm. Biomed. Anal.*, 2012, **67**, 201-208.

52 M. Liang, R. Liu, W. Qi, R. X. Su, Y. J. Yu, L. B. Wang and Z. M. He, *Food Chem.*, 2013, **138**, 1596-1603.

804 53 W. Peng, F. Ding, Y. T. Jiang and Y. K. Peng, *J. Agric. Food Chem.*, 2014, **62**, 2271-2283.

805 54 R. Gonçalves, N. Mateus and V. De Freitas, *J. Agric. Food Chem.*, 2010, **58**, 11924-11931.

806 55 Y. H. Chen, J. T. Yang and H. M. Martinez, *Biochemistry-US*, 1972, **11**, 4120-4131.

807 56 M. Hossain, A. Y. Khan and G. S. Kumar, *Plos One*, 2011, **6**, e18333.

808 57 O. Cala, F. Guillière and I. Krimm, *Anal. Bioanal. Chem.*, 2014, **406**, 943-956.

809 58 J. C. Chatham and J. R. Forder, *BBA-Gen. Subjects*, 1999, **1426**, 177-184.

810 59 Y. Liu, J. Lin, M. Chen and L. Song, *Food Chem. Toxicol.*, 2013, **58**, 264-272.

811 60 T. Wu, Q. Wu, S. Guan, H. Su and Z. Cai, *Biomacromolecules*, 2007, **8**, 1899-1906.

812

Table 1 Stern–Volmer Quenching Constants and Modified Stern–Volmer Quenching Constants for the Interaction between BSA and RA

T (K)	K_{SV} (10^4 L mol^{-1})	k_q (10^{12} L mol^{-1} s)$^{-1}$)	R^a	K_a (10^4 L mol^{-1})	R^a
288	7.48	7.48	0.9976	5.13	0.9999
298	6.66	6.66	0.9960	4.36	0.9994
308	5.07	5.07	0.9960	2.85	0.9995

[a] R is the correlation coefficient.

819

820

821 Table 2 Binding Parameters and Thermodynamic Parameters for BSA-RA System at

822 pH 7.4

T (K)	K (10^4 L mol^{-1})	n	R^a	ΔG^0 (kJ mol^{-1})	ΔH^0 (kJ mol^{-1})	ΔS^0 (J mol^{-1}K^{-1})
288	5.21	1.20	0.9992	-26.09		
298	4.18	1.26	0.9974	-26.21	-22.59	12.16
308	2.82	1.39	0.9954	-26.34		

823 [a] R is the correlation coefficient.

824

825

826

827 Table 3 Fluorescence Decay Fitting Parameters for the Interaction of BSA with RA

samples	τ_1 (ns)	A_1	τ_2 (ns)	A_2	χ^2	$<\tau>$ (ns)
Free BSA	5.40	0.498	7.32	0.502	0.997	6.19
BSA+RA (1:1)	3.96	0.258	6.78	0.742	1.077	6.05
BSA+RA (1:4)	2.49	0.171	6.22	0.829	1.028	5.58
BSA+RA (1:8)	1.55	0.171	5.75	0.829	1.083	5.03
BSA+RA (1:12)	1.14	0.228	5.27	0.772	1.080	4.33

828

829

830

831 Table 4. Three-Dimensional Fluorescence Spectral Characteristics of BSA-RA

832 System

peaks	BSA			BSA–RA		
	peak position λex/λem (nm/nm)	stokes Δλ (nm)	intensity *F*	peak position λex/λem (nm/nm)	stokes Δλ (nm)	intensity *F*
peak a	240/240→360/360	0	42.7→161.5	240/240→360/360	0	29.8→130.5
peak 1	280.0/347.0	67	888.2	280.0/351.5	71.5	489.8
peak 2	230.0/347.0	117	365.8	230.0/352.0	122	203.6

833

834

Figure Captions

Fig. 1 Molecular structure of rosmarinic acid.

Fig. 2 (A) Fluorescence quenching spectra of BSA by RA, 298 K, λ_{ex} = 280 nm. The concentration of BSA was fixed at 5.0×10^{-6} mol L^{-1}, and the concentration of RA (1-10) were 0, 0.5, 1.0, 1.5, 2.0, 2.5, 3.0, 4.0, 5.0 and 6.0×10^{-5} mol L^{-1}, respectively. Curve 0 represented the fluorescence emission spectrum of RA only. (B) The Stern–Volmer plots for the BSA-RA system at three different temperatures. (C) The Scatchard plots for the BSA-RA system. (D) Job's plot of fluorescence intensity changes as a function of molar fraction of the BSA-RA system.

Fig. 3 (A) Van't Hoff plot of BSA-RA system. (B) Effect of site markers probes on the fluorescence of the BSA−RA system (298 K, λ_{ex} = 280 nm). The concentrations of BSA and all the markers (warfarin, ibuprofen and digitoxin) were fixed at 5.0×10^{-6} mol L^{-1}. (C) Overlap between the fluorescence emission spectrum of BSA (1) and UV–vis absorption spectrum of RA (2), T = 298 K, pH = 7.40, λ_{ex} = 280 nm.

Fig. 4 (A) The time-resolved fluorescence decay of the BSA-RA system. (B) The Stern–Volmer curves for the intrinsic fluorescence quenching of the BSA-RA system.

Fig. 5 (A) Fluorescence quenching spectra of ANS bound BSA in the presence RA. C_{BSA} = 5.0×10^{-6} mol L^{-1}, C_{ANS} = 15.0×10^{-6} mol L^{-1} and the concentration of RA (1-10) were 0, 0.5, 1.0, 1.5, 2.0, 2.5, 3.0, 4.0, 5.0 and 6.0×10^{-5} mol L^{-1}, respectively. The inset showed the emission spectra of BSA only (1', 5.0×10^{-6} mol L^{-1}), RA only (2', 15.0×10^{-6} mol L^{-1}) and RA (3', 15.0×10^{-6} mol L^{-1})

incubated with ANS (15.0×10^{-6} mol L^{-1}) under the same experimental condition (λ_{ex} = 370 nm). (B) FT-IR spectra of free BSA (a) and difference spectra of BSA-RA system with the molar concentration ratio of BSA to RA of 1:4 in pH 7.4 phosphate buffer solution, $C_{BSA} = 1.0 \times 10^{-4}$ mol L^{-1}, $C_{RA} = 4.0 \times 10^{-4}$ mol L^{-1}.

Fig. 6 (A) Far-UV CD spectra of the BSA-RA system at room temperature. The concentration of BSA was fixed at 2.5×10^{-6} mol L^{-1} and the concentration of RA (1-5) were 0, 0.5, 1.0, 2.0 and 3.0×10^{-5} mol L^{-1}, respectively. (B) Near-UV CD spectra of BSA treated with various concentrations of RA. The concentration of BSA was fixed at 1.0×10^{-5} mol L^{-1} and the concentration of RA (1-4) were 0, 2.0, 4.0 and 6.0×10^{-5} mol L^{-1}, respectively.

Fig. 7 ^{1}H NMR spectra of RA at various molar ratios of RA to BSA. The concentration of RA was 2.5×10^{-3} mol L^{-1} and the concentrations of BSA (from top to bottom) were 0, 2.5×10^{-5} and 2.5×10^{-4} mol L^{-1}, respectively. Assignments were presented in the topmost spectra.

Fig. 8 The best energy ranked results of docking. (A) Binding site of RA on BSA. BSA was shown in cartoon. The domains were color-coded as follows: I, magenta; II, yellow; III, red. RA was represented using spheres. The atoms of RA were color-coded as follows: C, green; H, white; O, red. (B) The 2D representation showed the interaction between RA and its neighbouring residues. The pink circles represented the residues participating in hydrogen bonds, charge or polar interactions. The green circles were residues participating in van der Waals interactions. The light blue circle surrounding a given residue/atom denoted its solvent-accessible surface. (C) A surface diagram of BSA (spheres model) with RA (sticks model) was shown. The inset was the close-up view of

885 the predicted high-affinity pocket.

886 Fig. 9 (A) Time dependence of RMSD values for BSA and BSA-RA complex during
887 11 ns MD simulation. (B) The RMSF values of BSA-RA complex for each
888 residue. The residues located in the binding pocket flagged as gray bars.

889

890

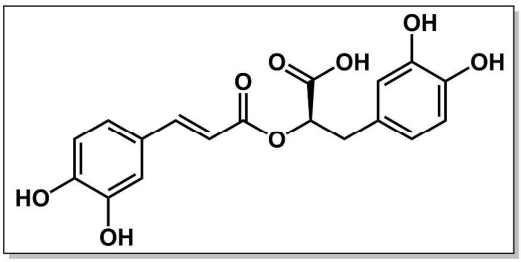

891

892

893 Fig. 1

894

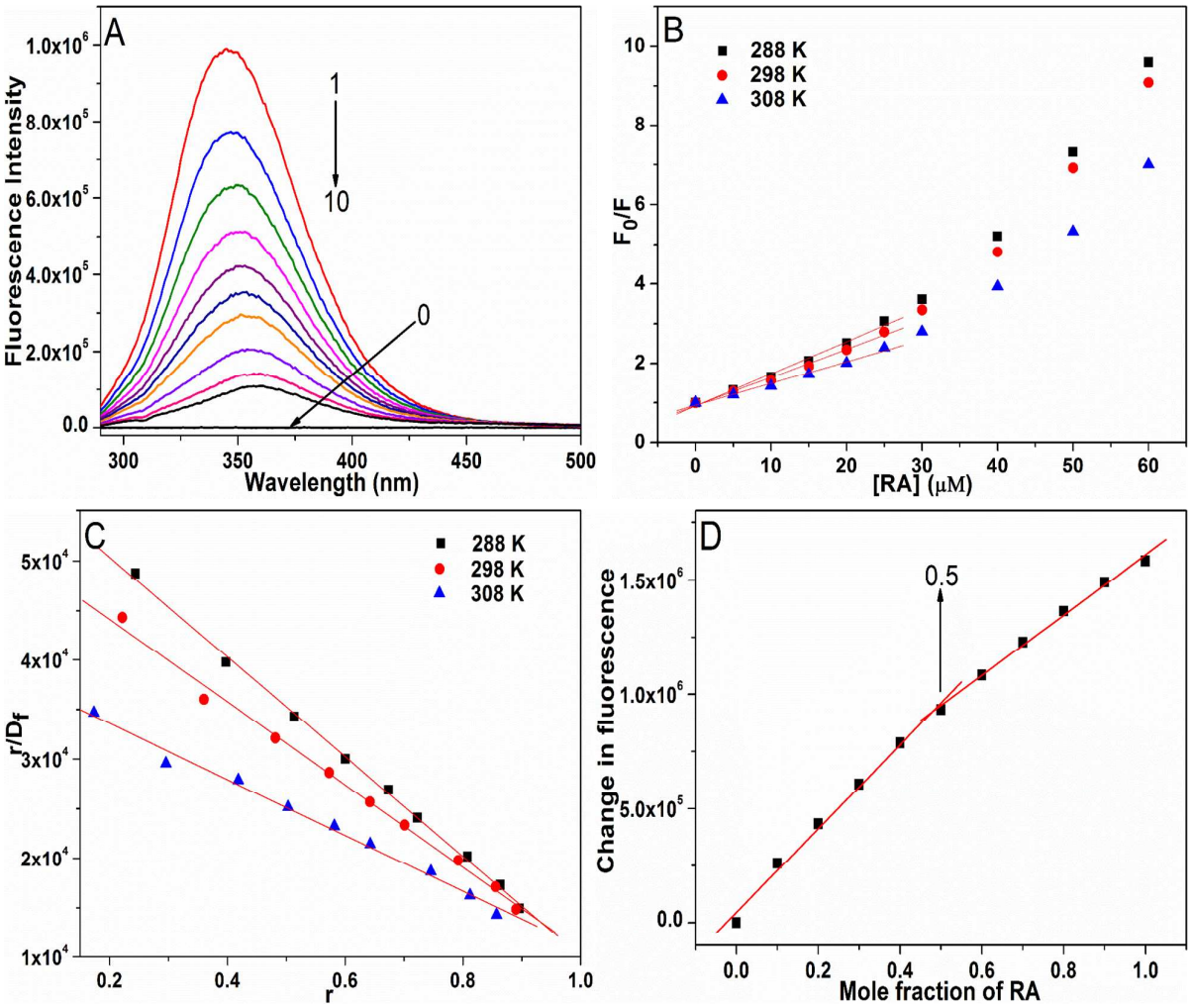

Fig. 2

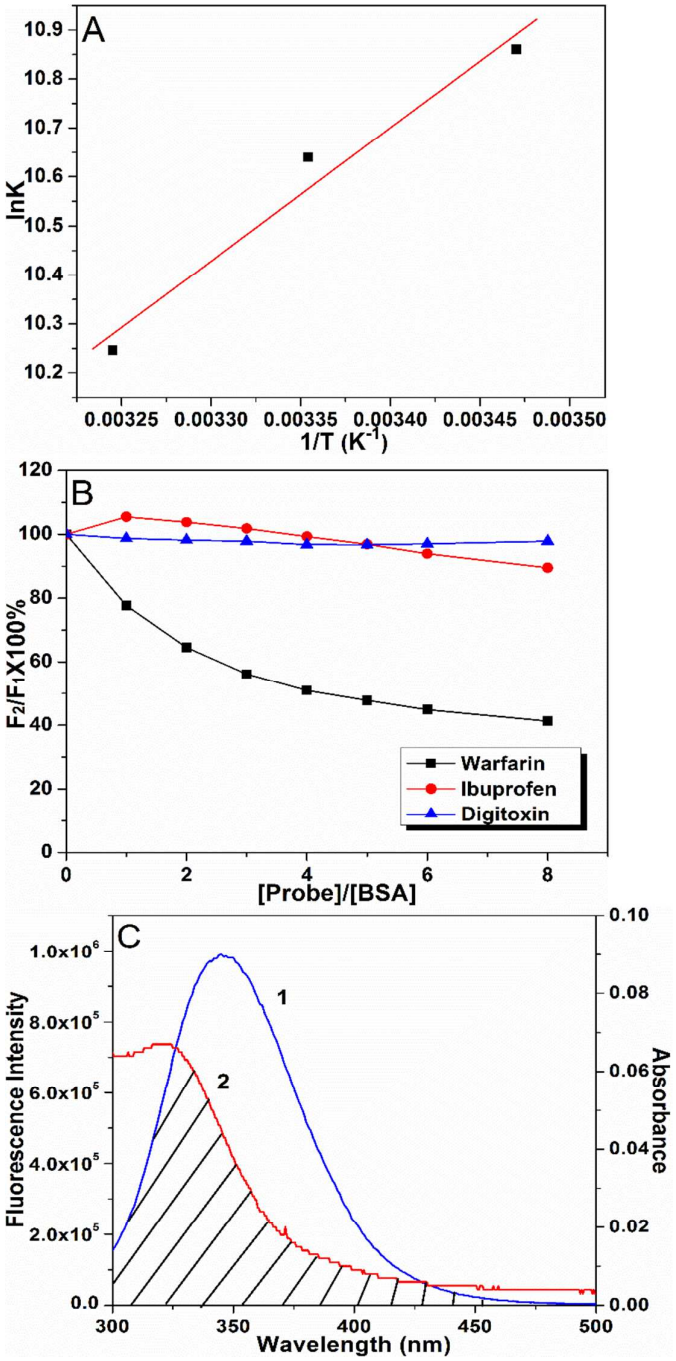

Fig. 3

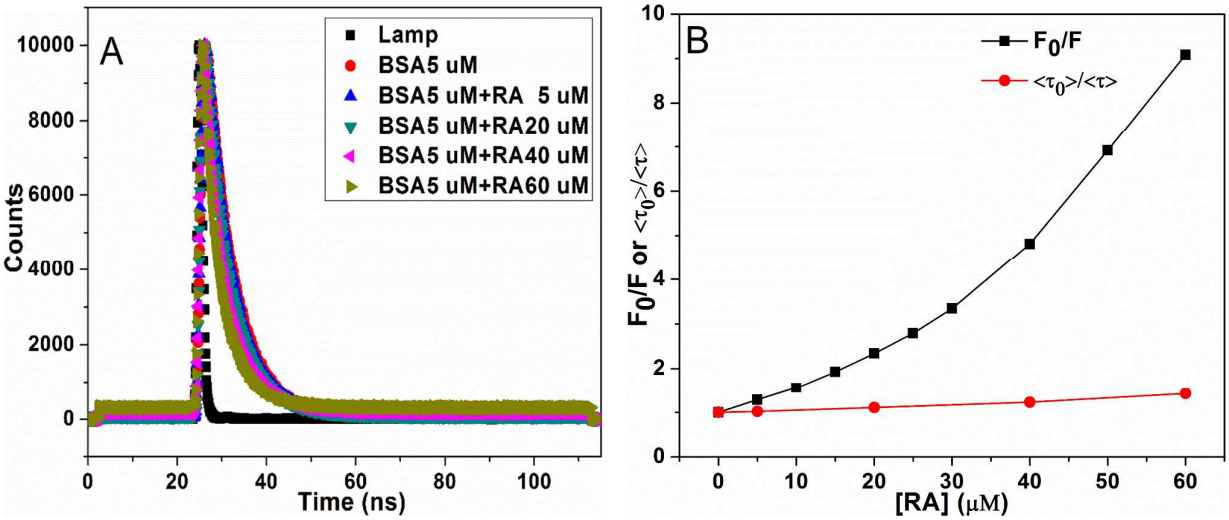

Fig. 4

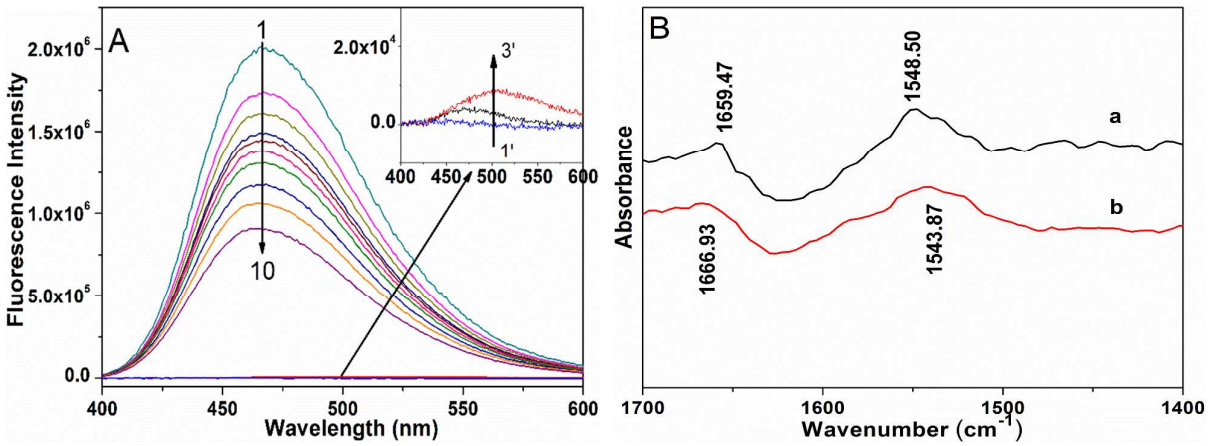

Fig. 5

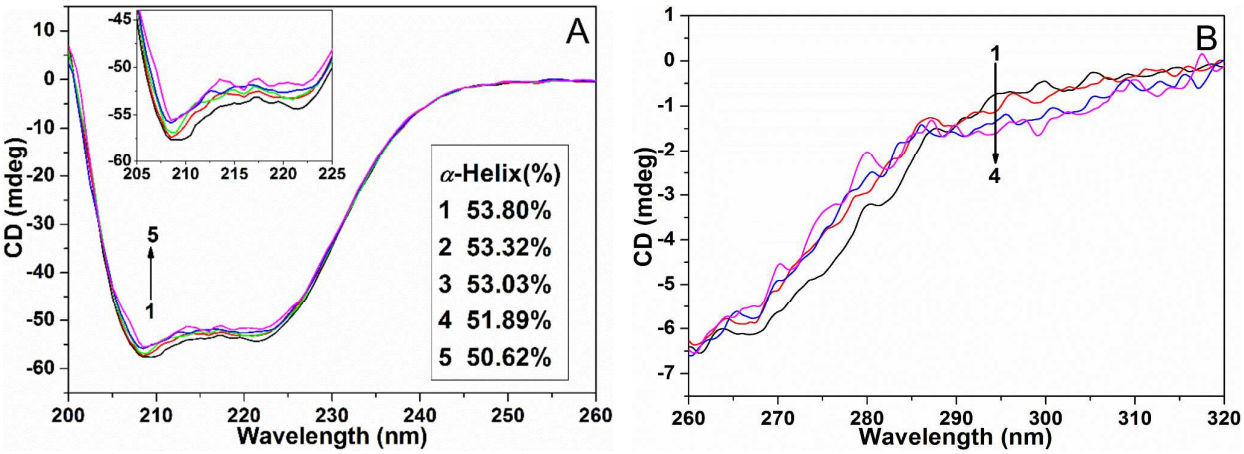

Fig. 6

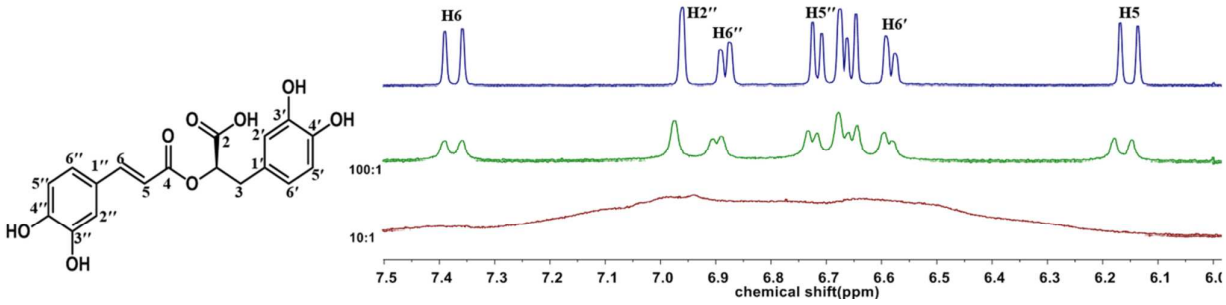

983

984

985 Fig. 7

986

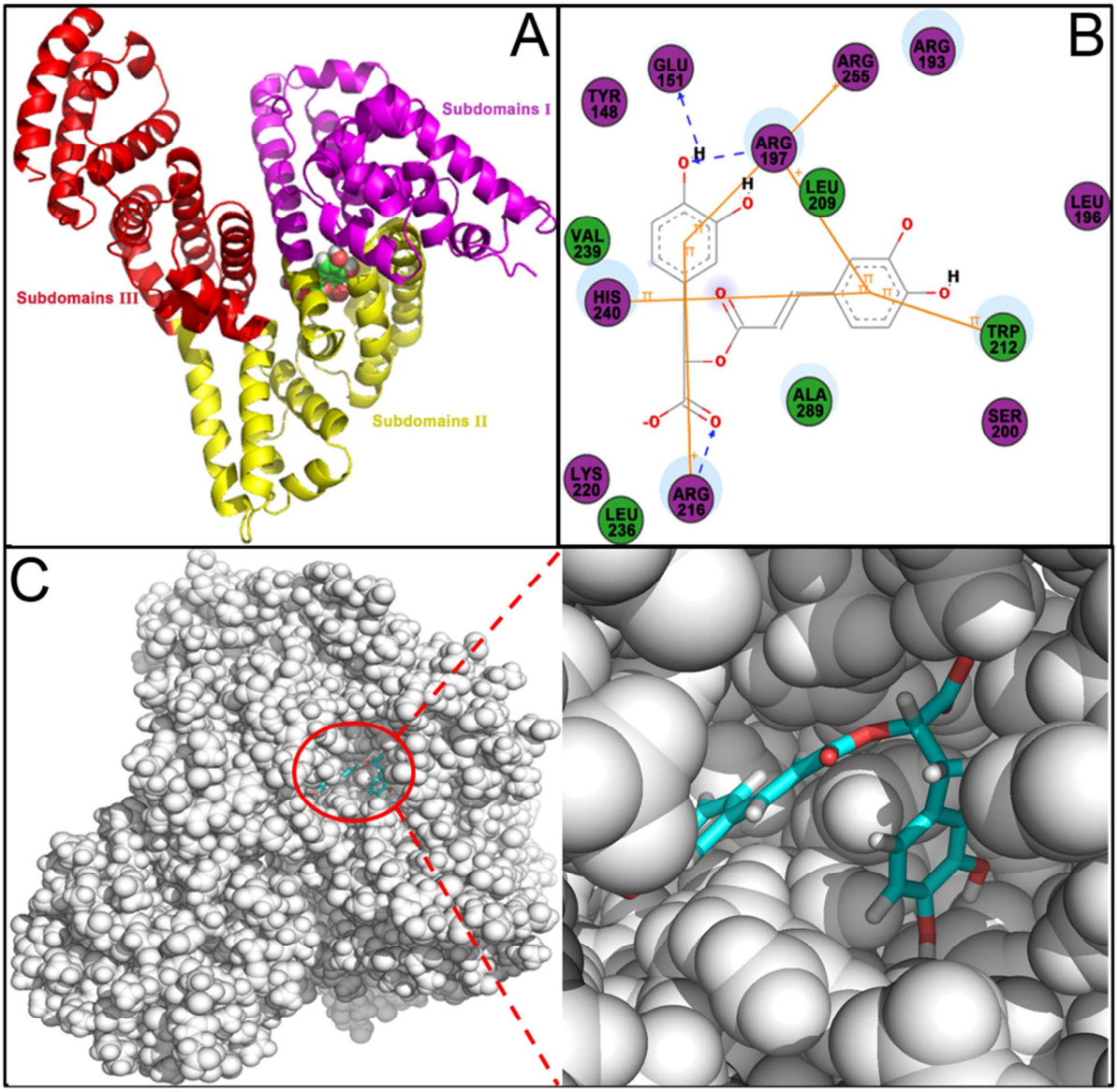

Fig. 8

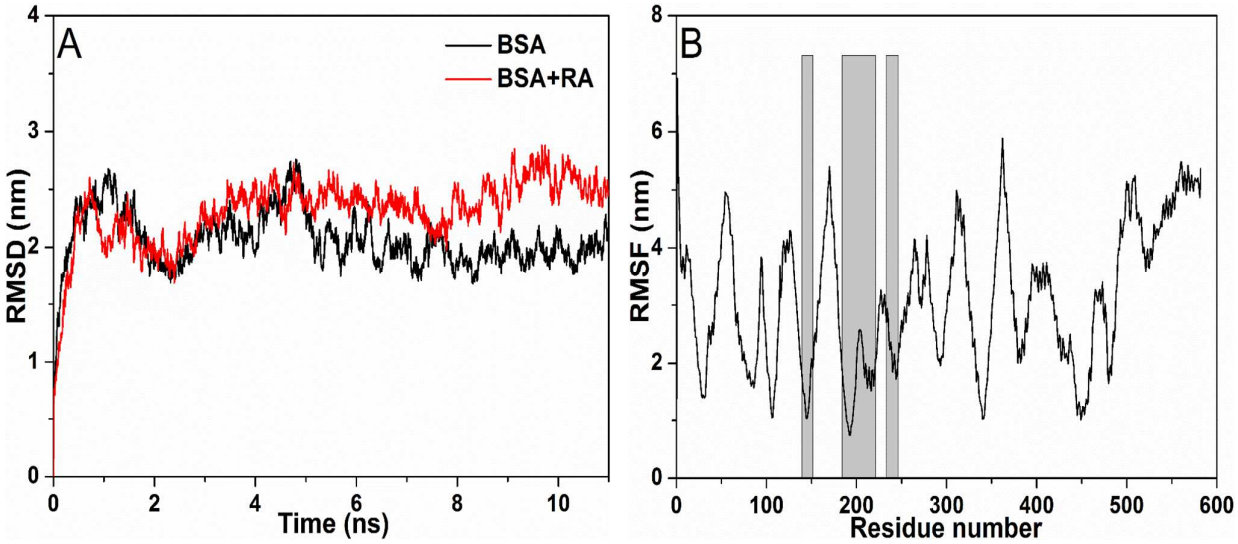

Fig. 9

1001

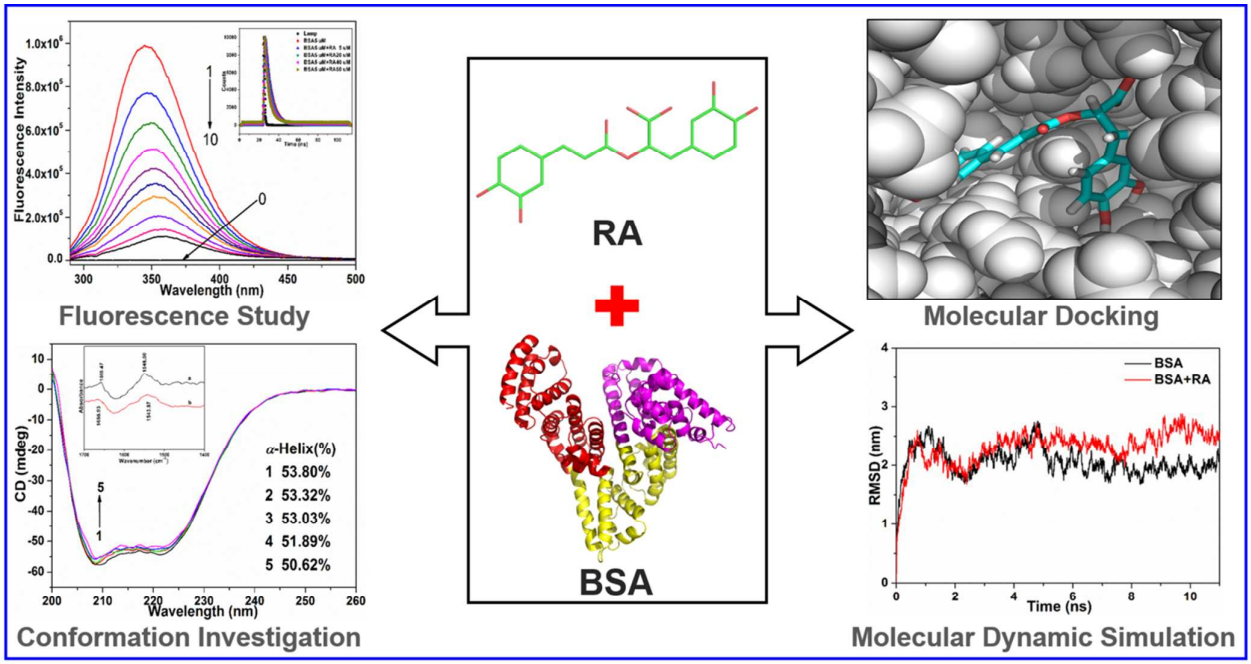

1002

1003

1004 TOC Graphic

1005